


**$E2$  decay characteristics of the  $M1$  scissors mode of  $^{152}\text{Sm}$** K. E. Ide <sup>1,\*</sup>, T. Beck <sup>1</sup>, V. Werner <sup>1</sup>, M. Berger <sup>1</sup>, S. W. Finch <sup>2</sup>, U. Friman-Gayer <sup>1,†</sup>, J. Kleemann <sup>1</sup>, Krishichayan,<sup>2</sup>  
B. Löher <sup>1</sup>, O. Papst <sup>1</sup>, N. Pietralla <sup>1</sup>, D. Savran <sup>3</sup>, W. Tornow,<sup>2</sup> M. Weinert <sup>4</sup>, J. Wiederhold <sup>1</sup> and A. Zilges <sup>4</sup><sup>1</sup>*Institut für Kernphysik Technische Universität Darmstadt, Schlossgartenstrasse 9, 64289 Darmstadt, Germany*<sup>2</sup>*Department of Physics, Duke University and Triangle Universities Nuclear Laboratory, Durham, North Carolina 27708-0308, USA*<sup>3</sup>*ExtreMe Matter Institute EMMI and Research Division, GSI Helmholtzzentrum für Schwerionenforschung, Planckstrasse 1, 64291 Darmstadt, Germany*<sup>4</sup>*Institut für Kernphysik Universität zu Köln, Zùlpicher Strasse 77, 50937 Köln, Germany*

(Received 3 June 2020; revised 15 March 2021; accepted 12 April 2021; published 6 May 2021)

The  $E2/M1$  multipole mixing ratio of the  $1_{sc}^+ \rightarrow 2_1^+$   $\gamma$ -ray transition and therefore the  $F$ -vector  $E2$  decay of the scissors mode of the shape-phase transitional nucleus  $^{152}\text{Sm}$  have been measured with the nuclear resonance fluorescence method at the High-Intensity  $\gamma$ -ray Source (HI $\gamma$ S). Furthermore, parity quantum numbers of several dipole-excited states have been remeasured, making use of the polarized  $\gamma$ -ray beam at HI $\gamma$ S, and partially reassigned. The new data enable an unambiguous determination of the proton and neutron effective boson quadrupole charges within the proton-neutron interacting boson model. With the well-constrained parameter set, a new mixed-symmetry state is predicted.

DOI: [10.1103/PhysRevC.103.054302](https://doi.org/10.1103/PhysRevC.103.054302)**I. INTRODUCTION**

Shape-phase transitions in chains of nuclei are often observed in rapid changes of isoscalar (IS) observables like the excitation energy ratio  $R_{4/2} = E_{4^+}/E_{2^+}$  or the electric quadrupole ( $E2$ ) transition strength  $B(E2; 2_1^+ \rightarrow 0_1^+)$  of the first excited  $2^+$  state of even-even nuclei. Such a rapid change of nuclear shapes from spherical to axially deformed is well-known for rare-earth isotopes around  $N = 90$  [1,2], e.g.,  $^{150}\text{Nd}$ ,  $^{152}\text{Sm}$ , and  $^{154}\text{Gd}$ . Another signature of a quantum phase transition (QPT) is the total magnetic dipole ( $M1$ ) transition strength of the scissors mode to the ground state, which correlates with the low-lying collective  $E2$  transition strength [3].

The scissors mode is, in general, an orbital out-of-phase oscillation of a coupled two-component many-body quantum system [4]. It is a low-lying magnetic dipole excitation in deformed nuclei, where it was predicted in 1978 by Lo Iudice and Palumbo [5] in the framework of the semiclassical two-rotor model of coupled quadrupole-deformed proton and neutron subsystems. In the proton-neutron interacting boson model (IBM-2) [6] it is predicted as a valence space excitation [7]. It was first discovered in the deformed nucleus  $^{156}\text{Gd}$  [8]. Within the IBM-2, the proton-neutron symmetry of the wave function is quantified by the  $F$ -spin quantum number [6], which is the bosonic analog of isospin for nucleons. The class

of lowest-energy mixed-symmetry states, which includes the scissors mode, is characterized by a  $F$ -spin quantum number of  $F = F_{\max} - 1$ , where  $F_{\max} = (N_{\pi} + N_{\nu})/2$  with the number of proton (neutron) bosons  $N_{\pi}$  ( $N_{\nu}$ ).

Due to the proton-neutron mixed-symmetric nature of the scissors mode, its  $M1$  transition strength to the proton-neutron symmetric ground state and its  $E2$  transition strength to the symmetric  $2_1^+$  state are isovector (IV) observables. In contrast to IS- $E2$  observables no impact of a QPT on IV- $E2$  observables has, so far, been demonstrated though it has been predicted by Otsuka and Ginocchio [9]. Only with the information of both, IS- and IV- $E2$  transition strengths, effective proton and neutron quadrupole charges can be determined for a given nucleus from data on its structure, alone.

Besides the above-mentioned  $M1$  strength of the scissors mode, indicators for a QPT in the mixed-symmetry sector could also be found in the location of the lowest  $2^+$  mixed-symmetry state and its IV- $E2$  excitation strength [10]. Data on the  $2_{ms}^+$  state toward deformed nuclei are sparse. Within the IBM-2, it is expected that the one-phonon  $2_{ms}^+$  excited state, which is known for many spherical nuclei well-below 3 MeV, evolves into a rotational state within the scissors mode's rotational band in deformed nuclei, around 3 MeV in the rare-earth region. However, only one potential observation of such a state in a nonspherical nucleus has so far been reported for  $^{156}\text{Gd}$  [11]. Therefore, there is no sufficient knowledge on its IV- $E2$  transition to the ground state across a spherical-deformed transition. Nevertheless, the scissors mode connects to the IS  $2_1^+$  state of the ground-state band via an IV- $E2$  transition, which is in competition to the  $1_{sc}^+ \rightarrow 2_1^+$   $M1$  decay.

It is the purpose of this work to determine  $E2$  decay strengths connecting the scissors mode of  $^{152}\text{Sm}$  to the ground-state band. This necessitates first a firm identification

\*kide@ikp.tu-darmstadt.de

†Present address: Department of Physics and Astronomy, University of North Carolina at Chapel Hill, Chapel Hill, NC 27599, USA; Triangle Universities Nuclear Laboratory, Duke University, Durham, NC 27708, USA.

of the fragmented scissors mode  $1^+$  states through an unambiguous parity measurement. The obtained data, combined with the recent data on  $^{156}\text{Gd}$ , will then serve to obtain IV and IS effective charges in the IBM-2, discussed with respect to the  $N \approx 90$  QPT.

## II. EXPERIMENT

Nuclear resonance fluorescence (NRF) experiments [12,13] with linearly polarized quasimonoenergetic  $\gamma$ -ray beams [14] have been performed at the High-Intensity  $\gamma$ -ray Source (HI $\gamma$ S) [15] at Duke University in Durham, North Carolina. The photon beams were impinged on a  $\text{Sm}_2\text{O}_3$  target, which contained 1.61387(7) g of samarium with an enrichment of 96.1% in  $^{152}\text{Sm}$ . The remaining percentages of the target composition arise from contaminations from other samarium isotopes,  $^{154}\text{Sm}$  (2.92%),  $^{150}\text{Sm}$  (0.24%),  $^{149}\text{Sm}$  (0.25%),  $^{148}\text{Sm}$  (0.23%),  $^{147}\text{Sm}$  (0.22%), and  $^{144}\text{Sm}$  (0.04%). These contributions are small and, hence, negligible at the sensitivity level of our experiment. The target, which was contained in a polyvinyl-chloride container, was mounted at the center of a detector array downstream of the  $\gamma^3$  setup [16]. The setup included four high-purity germanium (HPGe) detectors at a polar angle of  $\theta = 90^\circ$  with respect to the beam axis and at azimuthal angles  $\phi$  of  $0^\circ$ ,  $90^\circ$ ,  $180^\circ$ , and  $270^\circ$  with respect to the horizontal polarization plane of the beam. In NRF experiments dipole-excited states ( $1^\pi$ ,  $\pi = \pm$ ) are predominantly excited. The angular distribution of a  $0^+ \rightarrow 1^\pi \rightarrow 0^+$   $\gamma$  cascade excited via a linearly polarized  $\gamma$ -ray beam is described by [17]

$$W_{0^+ \rightarrow 1^\pi \rightarrow 0^+}(\phi, \theta = 90^\circ) = \frac{3}{4}[1 + \pi \cos(2\phi)]. \quad (1)$$

In Fig. 1 the angular distributions of  $\gamma$  rays from the decay of  $1^\pi$  states to the ground state are shown in the detector plane ( $\theta = 90^\circ$ ). The detector positions are sensitive to the angular distributions and a  $\gamma$ -ray asymmetry [14,18]

$$\epsilon = \frac{N_{\parallel} - N_{\perp}}{N_{\parallel} + N_{\perp}}, \quad (2)$$

can be determined directly from intensities  $N$  measured in ( $\parallel$ ) and perpendicular ( $\perp$ ) to the beam-polarization plane to deduce transition properties.

The experiment was performed with a central beam energy of 2.99(5) MeV. Around this energy, main fragments of the scissors mode of  $^{152}\text{Sm}$  were expected [19]. The quasimonoenergetic  $\gamma$ -ray beam has a small energy spread with a full width at half maximum of approximately 100 keV. Only states in the energy range of the beam were excited. Decays of these excited states to lower-lying excited states, so-called inelastic transitions, are visible below the excitation energy range (see Fig. 2).

The angular distribution for a  $0^+ \rightarrow 1^+ \rightarrow 2^+$  cascade is given by [17]

$$W_{0^+ \rightarrow 1^+ \rightarrow 2^+}(\phi, \theta = 90^\circ; \delta_{1 \rightarrow 2}) = 1 + \frac{3}{40} \left( \frac{1 + 6\sqrt{5}\delta_{1 \rightarrow 2} + 5\delta_{1 \rightarrow 2}^2}{1 + \delta_{1 \rightarrow 2}^2} \right) \times \left( \cos(2\phi) - \frac{1}{3} \right), \quad (3)$$

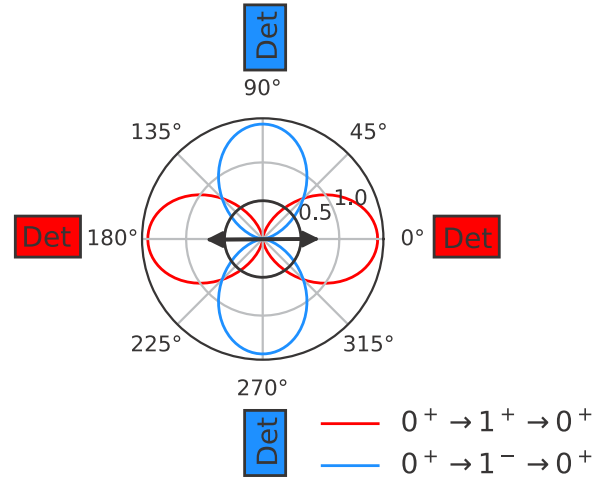


FIG. 1. Schematic detector setup along with the angular distributions of  $E1$  (blue) and  $M1$  (red) decay transitions of a photoexcited  $J = 1$  state to the  $0^+$  ground state are depicted in a plane perpendicular to the beam axis. The polarization of the impinging  $\gamma$ -ray beam is indicated by black arrows. The detector positions are optimized for the discrimination of both electromagnetic characters. The colors of the rectangles correspond to the sensitivity of the detectors to the angular distributions for positive (red) and negative (blue) parity of dipole-excited states.

with the  $E2/M1$  multipole mixing ratio  $\delta_{1 \rightarrow 2}$ , defined as

$$\delta_{1 \rightarrow 2} = \frac{\sqrt{3} E_\gamma \langle 2^+ || E2 || 1^+ \rangle}{10 \hbar c \langle 2^+ || M1 || 1^+ \rangle}, \quad (4)$$

in the phase convention of Krane *et al.* [17]. Following Eq. (3), the linear polarization of the incident photons causes an anisotropic azimuthal distribution of the scattered photons, which is sensitive to the  $E2/M1$  mixing ratio  $\delta_{1 \rightarrow 2}$  of the  $1^+_{sc} \rightarrow 2^+_1$  transition [11,20,21].

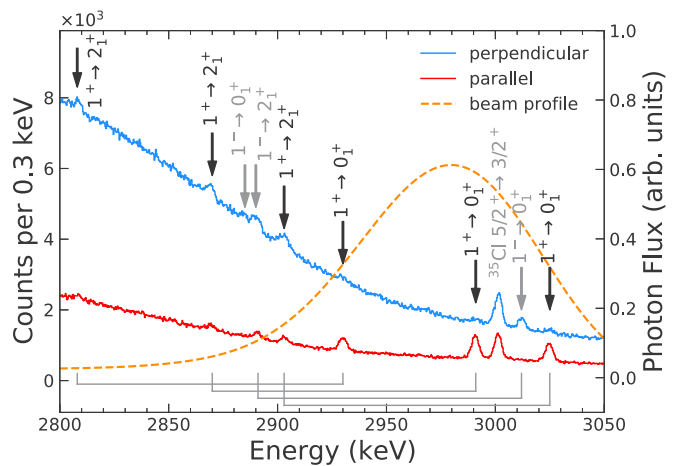


FIG. 2. Photon-scattering spectra of  $^{152}\text{Sm}$  taken at the HI $\gamma$ S facility [15]. The colors of the spectra correspond to Fig. 1. The energy profile of the beam is indicated by the dashed Gaussian curve (orange). Gray brackets below the spectra connect transitions from the same initial state.

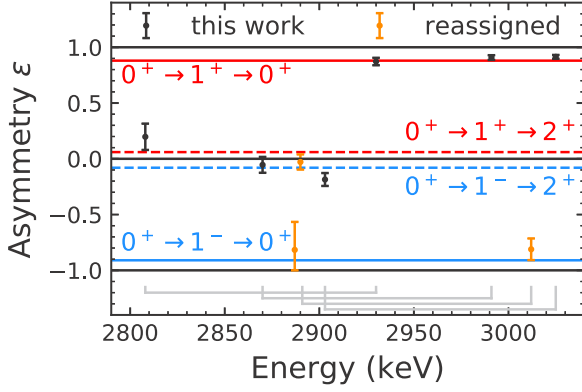


FIG. 3. Asymmetries of the observed transitions with their uncertainties (black, orange). The reassigned values of Ref. [19] are highlighted in orange. The ideal values 1 and  $-1$  are indicated for the asymmetries of a  $0^+ \rightarrow 1^+ \rightarrow 0^+$  cascade and  $0^+ \rightarrow 1^- \rightarrow 0^+$  cascade (black solid line), respectively. The expected values for the asymmetries taking into account the geometry of the setup are also shown. They amount to 0.88 for the  $0^+ \rightarrow 1^+ \rightarrow 0^+$  cascade (red solid line),  $-0.91$  for the  $0^+ \rightarrow 1^- \rightarrow 0^+$  cascade (blue solid line), 0.06 for the  $0^+ \rightarrow 1^+ \rightarrow 2^+$  cascade with  $\delta_{1 \rightarrow 2} = 0$  (red dashed line) and  $-0.08$  for the  $0^+ \rightarrow 1^- \rightarrow 2^+$  cascade (blue dashed line).

### III. RESULTS

In the  $\gamma$ -ray energy spectra shown in Fig. 2 a total of nine transitions of  $^{152}\text{Sm}$  can be distinguished. Besides the five transitions from dipole-excited states to the ground state, four transitions to the first excited  $2^+$  state at 121.8 keV [22] were observed. Further transitions, known from literature [19], are below the sensitivity of the present experiment and, hence, unobserved. The parity quantum numbers of the states were determined from the asymmetry [see Eq. (2)] of the respective ground-state decays. The asymmetries determined in this work for the observed transitions are shown in Fig. 3. The theoretical asymmetry of a  $0^+ \rightarrow 1^+ \rightarrow 0^+$  cascade is 1 and of a  $0^+ \rightarrow 1^- \rightarrow 0^+$  cascade is  $-1$ . Detector and target geometry results in attenuated values of 0.88 and  $-0.91$  for  $0^+ \rightarrow 1^+ \rightarrow 0^+$  and  $0^+ \rightarrow 1^- \rightarrow 0^+$  cascades, respectively, derived from GEANT4 [23–26] simulations. For a  $0^+ \rightarrow 1^+ \rightarrow 2^+$  cascade  $\epsilon = 0.06$  (red dashed line) and for a  $0^+ \rightarrow 1^- \rightarrow 2^+$  cascade  $\epsilon = -0.08$  (blue dashed line) are expected with the assumption that the multipole mixing ratio vanishes ( $\delta_{1 \rightarrow 2} = 0$ ).

From the obtained asymmetries, three states at energies of 2930, 2991, and 3025 keV are identified as  $1^+$  states, hence they will be interpreted as fragments of the scissors mode and two states at 2887 and 3012 keV are assigned  $J^\pi = 1^-$ . Previously, the transition at 2891 keV was assigned as a doublet from a ground-state transition of a  $1^+$  state, and a transition of a  $1^+$  state at 3012 keV to the  $2_1^+$  state [19,22]. In the present work, the 2891-keV transition is identified as a decay from the 3012-keV state only (see discussion below). The two  $1^-$  states at 3012 and 2887 keV were previously incorrectly assigned  $J^\pi = 1^+$  in the literature [19].

The previous (positive) parity assignment for the  $J = 1$  level at 3012 keV was based on a  $K$  quantum number assign-

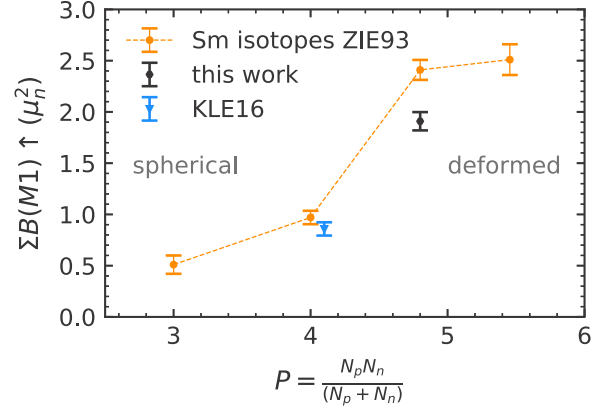


FIG. 4. Summed  $M1$  transition strength of stable samarium isotopes from Ziegler *et al.* [19] (orange squares). The orange dotted line is included to guide the eye over the QPT. Results from this work combined with values of Ziegler *et al.* for energy regions that were not studied here are represented by the black diamond. Remeasured values of  $^{150}\text{Sm}$  from Ref. [29] together with values of Ref. [19] are depicted by a blue triangle and which is slightly displaced with respect to the data point for the same isotope for better visibility.

ment from the decay branching ratio to the ground-state band [27] and on the rule of thumb that  $\Delta K = 1$   $E1$  transitions have comparatively low transition rates. Furthermore, the measured asymmetry of the 2891-keV transition is in good agreement with the expectation for a  $1^- \rightarrow 2^+$  transition, and excludes a significant contribution from a  $1^+ \rightarrow 0^+$  component. With the new parity assignment of the 3012-keV state, also the relative intensity of the 2891-keV transition of  $R_{\text{exp}} = \frac{B(E1; 1^\pi \rightarrow 2_1^+)}{B(E1; 1^\pi \rightarrow 0_1^+)} = 2.34^{+1.13}_{-1.22}$  is in good agreement with the Alaga expectation for a  $1_{K=0}^- \rightarrow 2^+$  transition of  $R_{\text{Alaga}} = 2$ .

The corrected parity assignments lead to a slight change in the summed low-lying  $M1$  transition strength of  $^{152}\text{Sm}$ , which changes from  $2.41(10) \mu_N^2$  in Ref. [19] to  $1.91(9) \mu_N^2$  from present data. The latter value is obtained from the results of this work combined with values from Ref. [19] for those energy regions that were outside the range of the present experiment. For the determination of the transition strengths we adopted the ground-state transition widths from Ziegler *et al.* [19], however, corrected for the branching ratios observed in the present work. The summed  $M1$  transition strengths of the isotopes  $^{148,150,152,154}\text{Sm}$  are shown as a function of the  $P$ -factor [28] in Fig. 4. The  $P$ -factor is defined as  $P = N_p N_n / (N_p + N_n)$  with  $N_p(N_n)$  the number of valence protons (neutrons).

It is noticeable that not all experimental asymmetry values for the inelastic decays from  $1^+$  states agree within their uncertainties with the limiting values for a multipole mixing ratio of zero. This indicates that these decays might not be of pure  $M1$  character, but potentially include an  $E2$  component.

The determination of the multipole mixing ratio is shown exemplarily for the transition of the  $1^+$  state at 2991 keV to the  $2_1^+$  state in Fig. 5. The asymmetry value and its uncertainty are projected onto the multipole mixing ratio axis via the expected dependence of the asymmetry on the

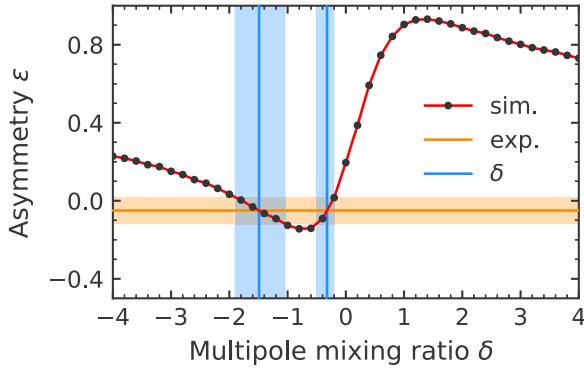


FIG. 5. Determination of the multipole mixing ratio  $\delta_{1\rightarrow 2}$  for the branching transition of the  $J^\pi = 1^+$  state at 2991 keV into the  $2_1^+$  state at 121.8 keV. The asymmetry values obtained from the GEANT4 simulation are shown as black circles interpolated by a red line. The experimental asymmetry and its uncertainty is depicted by the horizontal orange band. The multipole mixing ratio is given by the projection of the intersection point to the abscissa (blue).

multipole mixing ratio, which was simulated (black dots) with GEANT4 and interpolated (red line). The multipole mixing ratio is determined by the projection of the intersection of the experimental and simulated asymmetries (blue) yielding two solutions for  $\delta_{1\rightarrow 2}$ . The second solution for the multipole mixing ratio,  $\delta_{1\rightarrow 2} = -1.49^{+0.46}_{-0.42}$ , results in an  $E2$  transition strength of  $28.8^{+8.3}_{-5.4} e^2 \text{ fm}^4$ , but a very small  $M1$  transition strength of  $0.007^{+0.004}_{-0.002} \mu_N^2$ , untypical for the  $M1$  nature of the scissors mode and one order of magnitude smaller than the  $M1$  transition rate of that state to the ground state. Therefore, the solution close to zero  $\delta_{1\rightarrow 2} = -0.32^{+0.13}_{-0.19}$ , resulting in  $B(E2; 1^+_{\text{sc}} \rightarrow 2^+_1) = 6.0^{+8.5}_{-3.8} e^2 \text{ fm}^4$ , is favored. In addition, the otherwise resulting relatively large IV- $E2$  strengths would have been observed in previous electron scattering experiments [30]. The determined multipole mixing ratios as well as

the obtained  $E2$  transition strengths of the inelastic transitions of all scissors mode states studied here are listed in Table I. Also for the 2930-keV and 2991-keV  $1^+$  states, two solutions for the multipole mixing ratio  $\delta_{1\rightarrow 2}$  are possible and included in Table I.

In the following we use, except otherwise noted, the favoured solutions of  $\delta_{1\rightarrow 2}$  from Table I that exhibit dominant  $M1$  character.

#### IV. DISCUSSION

The summed  $E2$  transition strength of the inelastic transitions from the scissors mode to the  $2_1^+$  state observed in this work adds up to

$$\sum B(E2; 1^+_{\text{sc}} \rightarrow 2^+_1) = 60^{+14}_{-22} e^2 \text{ fm}^4 = 1.25^{+0.29}_{-0.50} \text{ W.u.},$$

which is a significant evidence for the  $E2$  decay of the scissors mode. Since  $^{152}\text{Sm}$  is a transitional nucleus for which no analytic equations exist as for the dynamical symmetries, the effective boson quadrupole charges are determined from a full IBM-2 calculation. For this purpose, the IBM-2 Hamiltonian [31]

$$\hat{H}_{\text{IBM-2}} = \epsilon(\hat{n}_{d_\pi} + \hat{n}_{d_\nu}) + \kappa(\hat{Q}_\pi^\chi + \hat{Q}_\nu^\chi) \cdot (\hat{Q}_\pi^\chi + \hat{Q}_\nu^\chi) + \hat{M}_{\pi\nu}, \quad (5)$$

where the quadrupole operator  $\hat{Q}_\rho^\chi$ ,  $\rho \in \{\pi, \nu\}$  is defined as

$$\hat{Q}_\rho^\chi = s_\rho^\dagger \tilde{d}_\rho + d_\rho^\dagger \tilde{s}_\rho + \chi_\rho [d_\rho^\dagger \tilde{d}_\rho]^{(2)}, \quad (6)$$

and the Majorana operator

$$\begin{aligned} \hat{M}_{\pi\nu} = & \frac{1}{2} \xi_2 (d_\nu^\dagger s_\pi^\dagger - d_\pi^\dagger s_\nu^\dagger) (\tilde{d}_\nu \tilde{s}_\pi - \tilde{d}_\pi \tilde{s}_\nu) \\ & + \sum_{k=1,3} \xi_k [d_\nu^\dagger d_\pi^\dagger]^{(k)} [\tilde{d}_\nu \tilde{d}_\pi]^{(k)}, \end{aligned} \quad (7)$$

TABLE I. Multipole mixing ratios, relative intensities  $I_\gamma^{\text{rel}}$  and reduced transition strengths of multipolarity  $\sigma L$  from dipole-excited states, which were determined in the present work.

$E_x^a$ (keV)	$E_\gamma^a$ (keV)	$\pi$	$I_\gamma^{\text{rel}}$	$\delta_{1\rightarrow 2}$	$\sigma 1$	$B(\sigma 1) \downarrow$	$\sigma 2$	$B(\sigma 2) \downarrow$
2887 <sup>b</sup>	2887	–	100		$E1$	$0.23(7) 10^{-3} e^2 \text{ fm}^2$		
2930	2930	+	100		$M1$	$0.146(13) \mu_N^2$		
	2808		$23_{-4}^{+5}$	$0.00^{+0.13}_{-0.13}$	$M1$	$0.038(8) \mu_N^2$	$E2$	$\leq 2.8 e^2 \text{ fm}^4$ <sup>d</sup>
	2808		$23_{-4}^{+5}$	$-3.56^{+1.24}_{-3.51}$	$M1$	$0.0028^{+0.0027}_{-0.0020} \mu_N^2$	$E2$	$65_{-9}^{+10} e^2 \text{ fm}^4$
2991	2991	+	100		$M1$	$0.087(14) \mu_N^2$		
	2870		$36.4_{-3.5}^{+4}$	$-0.32^{+0.13}_{-0.19}$	$M1$	$0.033(10) \mu_N^2$	$E2$	$6.0_{-3.8}^{+8.5} e^2 \text{ fm}^4$
	2870		$36.4_{-3.5}^{+4}$	$-1.49^{+0.46}_{-0.42}$	$M1$	$0.007^{+0.004}_{-0.002} \mu_N^2$	$E2$	$28.8_{-5.4}^{+8.3} e^2 \text{ fm}^4$
3012 <sup>b</sup>	3012	–	100		$E1$	$0.77(27) 10^{-3} e^2 \text{ fm}^2$		
	2891 <sup>c</sup>		$209_{-18}^{+19}$	$0.07^{+0.07}_{-0.07}$	$E1$	$1.8_{-0.7}^{+0.6} 10^{-3} e^2 \text{ fm}^2$	$M2$	$124_{-124}^{+512} \mu_N^2 \text{ fm}^2$
3025	3025	+	100		$M1$	$0.140(12) \mu_N^2$		
	2903		$52.3_{-3.3}^{+3.5}$	$-0.8_{-0.15}^{+0.25}$	$M1$	$0.050^{+0.020}_{-0.012} \mu_N^2$	$E2$	$54_{-25}^{+19} e^2 \text{ fm}^4$

<sup>a</sup>Taken from Ref. [22].

<sup>b</sup>Parity reassigned compared to Ref. [19].

<sup>c</sup>Formerly reported as an elastic transition.

<sup>d</sup>Limit corresponding to two standard deviations.



TABLE II. Experimental values for excitation energies,  $E_x$ , and transition strengths compared to IBM-2 results.

Observable	Experimental	IBM-2
$E_x(2_1^+)$ [MeV]	0.122 <sup>a</sup>	0.122
$E_x(4_1^+)$ [MeV]	0.366 <sup>a</sup>	0.366
$E_x(0_2^+)$ [MeV]	0.685 <sup>a</sup>	0.686
$E_x(2_2^+)$ [MeV]	0.810 <sup>a</sup>	0.905
$E_x(2_3^+)$ [MeV]	1.086 <sup>a</sup>	1.060
$E_x(1_{sc}^+)$ [MeV]	2.983(7) <sup>b</sup>	2.981
$E_x(2_{ms}^+)$ [MeV]	–	3.045
$B(E2; 2_1^+ \rightarrow 0_1^+)$ [W.u.]	145.0(16) <sup>a</sup>	145.0
$B(E2; 4_1^+ \rightarrow 2_1^+)$ [W.u.]	209.5(22) <sup>a</sup>	213.1
$B(E2; 0_2^+ \rightarrow 2_1^+)$ [W.u.]	33.3(12) <sup>a</sup>	38.9
$B(E2; 1_{sc}^+ \rightarrow 2_1^+)$ [W.u.]	1.25 <sup>+0.29</sup> <sub>-0.50</sub> <sup>c</sup>	1.25 <sup>c</sup>
$B(E2; 2_{ms}^+ \rightarrow 0_1^+)$ [W.u.]	–	0.48 <sup>c</sup>
$B(M1; 1_{sc}^+ \rightarrow 0_1^+)$ [ $\mu_N^2$ ]	0.373(23) <sup>c</sup>	0.371 <sup>c</sup>
$B(M1; 1_{sc}^+ \rightarrow 2_1^+)$ [ $\mu_N^2$ ]	0.121(24) <sup>c</sup>	0.260 <sup>c</sup>
$B(M1; 2_{ms}^+ \rightarrow 2_1^+)$ [ $\mu_N^2$ ]	–	0.69 <sup>c</sup>
$B(E2; 1_{sc}^+ \rightarrow 2_1^+)$ [W.u.]	2.13 <sup>+0.49</sup> <sub>-0.85</sub> <sup>d</sup>	2.12 <sup>d</sup>
$B(E2; 2_{ms}^+ \rightarrow 0_1^+)$ [W.u.]	–	0.81 <sup>d</sup>
$B(M1; 1_{sc}^+ \rightarrow 0_1^+)$ [ $\mu_N^2$ ]	0.636(30) <sup>e</sup>	0.637 <sup>d</sup>
$B(M1; 1_{sc}^+ \rightarrow 2_1^+)$ [ $\mu_N^2$ ]	0.298(31) <sup>f</sup>	0.448 <sup>d</sup>
$B(M1; 2_{ms}^+ \rightarrow 2_1^+)$ [ $\mu_N^2$ ]	–	1.19 <sup>d</sup>

<sup>a</sup>From Ref. [22].

<sup>b</sup> $B(M1; 1^+ \rightarrow 0_1^+)$ -weighted energy of the scissors mode from this work and Ziegler *et al.*

<sup>c</sup>Only transitions observed in the present work.

<sup>d</sup>Scaled to the total  $M1$  strength of the scissors mode (see text).

<sup>e</sup>Summation of the total  $M1$  strength attributed to the scissors mode from the literature [19] and corrected by our new data if applicable.

<sup>f</sup>Summation of the total  $B(M1; 1^+ \rightarrow 2_1^+)$  strength attributed to the scissors mode from the literature [19] with an assumed  $\delta_{1 \rightarrow 2} = 0$  and corrected by our new data if applicable.

is used. In Eqs. (5), (6), and (7),  $\hat{n}_d$  denotes the  $d$ -boson number operator, and  $s_\rho^\dagger(s_\rho)$  and  $d_\rho^\dagger(\tilde{d}_\rho)$  the  $s$ - and  $d$ -boson creation (annihilation) operators. The IBM-2 Hamiltonian is adjusted to the low-lying level scheme of  $^{152}\text{Sm}$  and the  $B(M1; 1_{sc}^+ \rightarrow 0_1^+)$ -weighted average of the energy of the scissors mode from this work and Ziegler *et al.* [19] (see Table II), as defined in Ref. [32],

$$\bar{E}(1_{sc}^+) = \frac{\sum_i E_i B(M1)_i}{\sum_i B(M1)_i} = 2983(7) \text{ keV}. \quad (8)$$

The parameters  $\epsilon$ ,  $\kappa$  and  $\chi$  have been adjusted to the low-energy level scheme, and the Majorana parameters  $\xi_i$  to the scissors mode, which results in the parameter set  $\epsilon_d = 0.473$  MeV,  $\kappa = -0.01938$  MeV,  $\xi_2 \equiv \frac{1}{2}\xi_{1,3} = 0.542$  MeV and  $\chi = -1.0589$ .

The transition operators are defined as

$$T^{(M1)} = \sqrt{\frac{3}{4\pi}} (g_\nu L_\nu + g_\pi L_\pi) \mu_N, \quad (9)$$

$$T^{(E2)} = e_\pi \hat{Q}_\pi^\chi + e_\nu \hat{Q}_\nu^\chi, \quad (10)$$

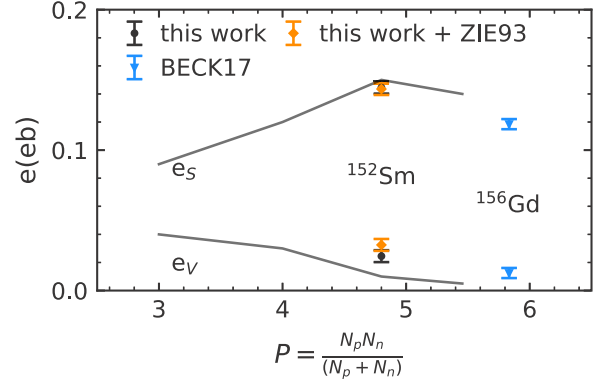


FIG. 6. Effective  $F$ -scalar and  $F$ -vector boson quadrupole charges as a function of the  $P$ -factor for the values obtained from transitions observed within this work (black) and rescaled to the total scissors  $M1$  strength (see text, orange) for  $^{152}\text{Sm}$  and the values from Beck *et al.* for  $^{156}\text{Gd}$  (blue). Predictions are from Ref. [9] (gray lines).

where  $L_\rho = \sqrt{10}[d_\rho^\dagger \tilde{d}_\rho]^{(1)}$ , is the angular momentum operator, and  $g_\rho$  is the effective boson  $g$ -factor with  $F$ -spin character  $\rho$ . For the  $E2$  transition operator the consistent  $Q$  formalism [33,34] is used and  $e_\rho$  denotes the effective boson quadrupole charges.

For the calculation of absolute  $B(M1)$  transition strengths, the effective  $g$ -factor difference was adjusted to the summed  $B(M1)$  strength of the scissors mode observed in this work of  $0.373(23) \mu_N^2$  resulting in  $(g_\pi - g_\nu) = 1.045 \mu_N$ . This value sets the scale for all  $F$ -vector  $M1$  transitions to states with maximum  $F$ -spin, including the branching transitions to the  $2_1^+$  state of the ground-state rotational band.

The effective boson quadrupole charges were adjusted to the IS  $B(E2; 2_1^+ \rightarrow 0_1^+)$  and the IV  $B(E2; 1_{sc}^+ \rightarrow 2_1^+)$  values. This yields the values of the effective quadrupole charges of  $e_\pi = 0.169$  eb and  $e_\nu = 0.120$  eb. Another representation of the results are the so-called  $F$ -scalar and  $F$ -vector boson charges,  $e_{S,V} = \frac{1}{2}(e_\pi \pm e_\nu)$ . They are shown in Fig. 6, where  $F$ -scalar and  $F$ -vector boson charges are plotted as a function of the  $P$ -factor. Besides the values of  $^{152}\text{Sm}$  also the  $F$ -scalar and  $F$ -vector boson charges of  $^{156}\text{Gd}$  [11] and predictions for the isotopes  $^{148,150,152,154}\text{Sm}$  [9] are shown.

The experimental data used for the adjustment of the parameters of the IBM-2 Hamiltonian are shown in Table II along with the IBM-2 predictions. The reproduction of the excitation energies is satisfactory. Also the  $E2$  transition strengths are in good agreement with the data. Let us turn to the  $E2$  properties of the scissors mode.

The  $B(M1; 1_{sc}^+ \rightarrow 0_1^+)$  strength of the  $1^+$  states observed in the present work adds up to  $0.373(23) \mu_N^2$ , hence, 41% of the experimentally known scissors mode  $M1$  strength of  $^{152}\text{Sm}$  has not been excited in the present experiment which was sensitive to a narrow energy region around 3 MeV, only. To obtain the full scissors mode  $M1$  strength from the calculation, the effective boson  $g$ -factor difference  $(g_\pi - g_\nu) \approx 1.37 \mu_N$  needs to be chosen. If we assume the same factor for the missed  $B(E2; 1_{sc}^+ \rightarrow 2_1^+)$  strength, then a total IV- $E2$  strength

of  $2.13^{+0.49}_{-0.85}$  W.u. fragmented over  $1^+$  states in the energy range of 2.7–3.7 MeV would be expected. Scaling  $e_{\pi,\nu}$  accordingly in the IBM-2, results in values of  $e_{\pi} = 0.176$  eb and  $e_{\nu} = 0.111$  eb. Resulting  $e_{S,\nu}$  charges are included in Fig. 6, qualitatively not changing the overall picture.

If one uses the  $E2$ -dominated solutions for the  $\delta_{1\rightarrow 2}$  values from Table I, then the scaled total  $1^+ \rightarrow 2^+$   $E2$ -strength would amount to  $5.64^{+0.67}_{-1.06}$  W.u. Even if this value is used, the respective IV boson charges in Fig. 6 would increase only less than a factor of two, and the qualitative discussion remains unchanged.

The energy of the  $2^+_{\text{ms}}$  state is predicted at 3045 keV, which is above the  $1^+$  scissors mode state, in comparison to spherical nuclei, where the  $2^+_{\text{ms}}$  is the lowest mixed-symmetry state. In this energy region no  $2^+$  state as a candidate for the  $2^+_{\text{ms}}$  is known [22]. The only possible candidate in this region could be a recently reported [35] energy level at 3039.1 keV lacking a spin-parity assignment. Also, the energy of this state agrees with the IBM-2 prediction. Its calculated transition strength to the ground state and to the  $2^+_1$  state are included in Table II. The latter resemble closely the recent observations in  $^{156}\text{Gd}$  [11] with an estimated transition strength of  $B(M1; 2^+_{\text{sc}} \rightarrow 2^+_1) = 0.74(6)\mu_N^2$  based on an Alaga-rule constraint.

Finally, we concede that the calculated  $M1$  transition strength of the  $1^+_{\text{sc}}$  scissors mode to the first  $2^+$  state exceeds the experimental value by about 50%. While the ratio of the summed  $M1$  strength from the scissors mode to the  $2^+_1$  state to the summed  $M1$  strength from the scissors mode to the ground state (see bottom of Table II) amounts experimentally to 47(5)%, our IBM-2 fit yields a larger value of 70%. It is not obvious how this discrepancy can be resolved while maintaining the description of the structural character of  $^{152}\text{Sm}$  as being located close to the critical point of the spherical-to-axially deformed shape-phase transition. The very small  $M1$  transition strengths between low-energy levels established experimentally [22] imply the absence of significant  $F$ -spin mixing at low energies.  $M1$  transitions from the  $1^+$  scissors mode with  $F$ -spin  $F = F_{\text{max}} - 1$  to all low-energy levels are thus proportional to  $(g_{\pi} - g_{\nu})^2$  and cannot be varied independently by different choices for the effective boson  $g$ -factors in the calculation. Varying the structural parameter  $\zeta = 4N_B/(4N_B - \epsilon/\kappa)$  [1] for different choices of the structural parameter  $\chi$  indicates that the calculated branching ratio of the scissors mode to the  $2^+_1$  state as compared to the ground state always exceeds the Alaga value of 0.5 along the entire U(5)-to-SU(3) structural path.

Figure 7 displays the results for this  $M1$  branching ratio for various choices of parameters of the Hamiltonian (5). Also the consideration of a  $d$ -boson anharmonicity  $\propto \hat{n}_d^2$  does not resolve this discrepancy. A more complete study of the entire parameter space of the IBM-2 might be needed for deciding the question if a description of this  $M1$  branching ratio, consistent with the structure of the low-energy levels,

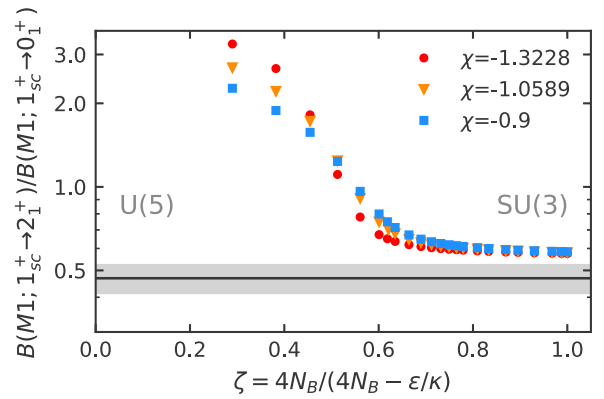


FIG. 7.  $\frac{B(M1; 1^+_{\text{sc}} \rightarrow 2^+_1)}{B(M1; 1^+_{\text{sc}} \rightarrow 0^+_1)}$  ratio as a function of  $\zeta$  for different values of  $\chi$  is depicted logarithmically. The experimental value and its uncertainty is indicated by the horizontal line. For a U(5) spherical configuration ( $\zeta = 0$ ) the  $M1$  branching ratio is undefined since both transitions are forbidden. Notably, the ratio never goes below the experimental value and equals the Alaga value of 0.5 modified by the effects of the finite boson number in the SU(3)-limit ( $\zeta = 1$ ).

can be obtained in the IBM-2, or not. This is certainly beyond the scope of this article.

## V. SUMMARY

A highly sensitive NRF measurement with a quasi-monoenergetic, polarized  $\gamma$ -ray beam has been performed to study the scissors mode of the phase transitional nucleus  $^{152}\text{Sm}$ . Within the uncertainty nonzero multipole mixing ratios of the  $\gamma$ -ray transitions from the scissors mode to the  $2^+_1$  state have been measured. It was possible to determine the value for the  $B(E2; 1^+_{\text{sc}} \rightarrow 2^+_1)$  of  $^{152}\text{Sm}$ . With this  $F$ -vector transition and the  $F$ -scalar low-lying  $E2$  transition strengths the effective boson quadrupole-charges were determined in the framework of the IBM-2 and reflect the expected behavior at the phase transition. The energy and transition strength of the  $2^+_{\text{ms}}$  state is predicted within the IBM-2 by an adjustment of the values for the low-energy level scheme and the measured  $1^+$  scissors mode states of  $^{152}\text{Sm}$ . This yields the expected change of the predicted position of the  $2^+_{\text{ms}}$  state from below the  $1^+_{\text{sc}}$  state in spherical nuclei to a part of the rotational band of the scissors mode in deformed nuclei.

## ACKNOWLEDGMENTS

The authors thank the HI $\gamma$ S accelerator crew for providing perfect experimental conditions. This work was funded by the Deutsche Forschungsgemeinschaft–Project ID No. 279384907-SFB 1245, partly by the BMBF under Grants No. 05P15RDEN9, No. 05P18RDEN9, and No. 05P2018PKEN9, by the State of Hesse under the Grant “Nuclear Photonics” within the LOEWE program U.S. DOE Grant No. DE-FG02-97ER41033.

- [1] R. F. Casten, *Nat. Phys.* **2**, 811 (2006).
- [2] R. F. Casten, *Prog. Part. Nucl. Phys.* **62**, 183 (2009).
- [3] N. Pietralla, P. von Brentano, R.-D. Herzberg, U. Kneissl, J. Margraf, H. Maser, H. H. Pitz, and A. Zilges, *Phys. Rev. C* **52**, R2317 (1995).
- [4] K. Heyde, P. von Neumann-Cosel, and A. Richter, *Rev. Mod. Phys.* **82**, 2365 (2010).
- [5] N. Lo Iudice and F. Palumbo, *Phys. Rev. Lett.* **41**, 1532 (1978).
- [6] T. Otsuka, A. Arima, and F. Iachello, *Nucl. Phys. A* **309**, 1 (1978).
- [7] F. Iachello, *Nucl. Phys. A* **358**, 89 (1981).
- [8] D. Bohle, A. Richter, W. Steffen, A. E. L. Dieperink, N. L. Iudice, F. Palumbo, and O. Scholten, *Phys. Lett. B* **137**, 27 (1984).
- [9] T. Otsuka and J. N. Ginocchio, *Phys. Rev. Lett.* **54**, 777 (1985).
- [10] N. Pietralla, P. von Brentano, and A. F. Lisetskiy, *Prog. Part. Nucl. Phys.* **60**, 225 (2008).
- [11] T. Beck, J. Beller, N. Pietralla, M. Bhike, J. Birkhan, V. Derya, U. Gayer, A. Hennig, J. Isaak, B. Löher *et al.*, *Phys. Rev. Lett.* **118**, 212502 (2017).
- [12] U. Kneissl, H. H. Pitz, and A. Zilges, *Prog. Part. Nucl. Phys.* **37**, 349 (1996).
- [13] U. Kneissl, N. Pietralla, and A. Zilges, *J. Phys. G* **32**, R217 (2006).
- [14] N. Pietralla, H. R. Weller, V. N. Litvinenko, M. W. Ahmed, and A. P. Tonchev, *Nucl. Instrum. Meth. A* **483**, 556 (2002).
- [15] H. R. Weller, M. W. Ahmed, H. Gao, W. Tornow, Y. K. Wu, M. Gai, and R. Miskimen, *Prog. Part. Nucl. Phys.* **62**, 257 (2009).
- [16] B. Löher, V. Derya, T. Aumann, J. Beller, N. Cooper, M. Duchêne, J. Endres, E. Fiori, J. Isaak, J. Kelley *et al.*, *Nucl. Instrum. Meth. A* **723**, 136 (2013).
- [17] K. S. Krane, R. M. Steffen, and R. M. Wheeler, *At. Data Nucl. Data Tables* **11**, 351 (1973).
- [18] N. Pietralla, Z. Berant, V. N. Litvinenko, S. Hartman, F. F. Mikhailov, I. V. Pinayev, G. Swift, M. W. Ahmed, J. H. Kelley, S. O. Nelson *et al.*, *Phys. Rev. Lett.* **88**, 012502 (2001).
- [19] W. Ziegler, N. Huxel, P. von Neumann-Cosel, C. Rangacharyulu, A. Richter, C. Spieler, C. De Coster, and K. Heyde, *Nucl. Phys. A* **564**, 366 (1993).
- [20] N. Pietralla, M. W. Ahmed, C. Fransen, V. N. Litvinenko, A. P. Tonchev, and H. R. Weller, *AIP Conf. Proc.* **656**, 365 (2003).
- [21] G. Rusev, A. P. Tonchev, R. Schwengner, C. Sun, W. Tornow, and Y. K. Wu, *Phys. Rev. C* **79**, 047601 (2009).
- [22] M. J. Martin, *Nucl. Data Sheets* **114**, 1497 (2013).
- [23] S. Agostinelli, J. Allison, K. Amako, J. Apostolakis, H. Araujo, P. Arce, M. Asai, D. Axen, S. Banerjee, G. Barrand *et al.*, *Nucl. Instrum. Meth. A* **506**, 250 (2003).
- [24] J. Allison, K. Amako, J. Apostolakis, H. Araujo, P. Arce Dubois, M. Asai, G. Barrand, R. Capra, S. Chauvie, R. Chytracsek *et al.*, *IEEE T. Nucl. Sci.* **53**, 270 (2006).
- [25] J. Allison, K. Amako, J. Apostolakis, P. Arce, M. Asai, T. Aso, E. Bagli, A. Bagulya, S. Banerjee, G. Barrand *et al.*, *Nucl. Instrum. Meth. A* **835**, 186 (2016).
- [26] U. Friman-Gayer, J. Kleemann, and O. Papst, GEANT4 simulation of the Upstream Target Room (UTR) at the HI $\gamma$ S facility (2019), <https://doi.org/10.5281/zenodo.3430154>.
- [27] G. Alaga, K. Alder, A. Bohr, and B. R. Mottelson, K. Dan. Vidensk. Selsk. Mat. Fys. Medd. **29**, 1 (1955).
- [28] R. F. Casten, D. S. Brenner, and P. E. Haustein, *Phys. Rev. Lett.* **58**, 658 (1987).
- [29] J. Kleemann, B.Sc. Thesis, Technische Universität Darmstadt, 2016.
- [30] A. Nitsch, Diplomarbeit, Technische Universität Darmstadt, 1991, [https://inis.iaea.org/search/search.aspx?orig\\_q=RN:17033326](https://inis.iaea.org/search/search.aspx?orig_q=RN:17033326).
- [31] T. Otsuka and N. Yoshida, User's manual of the program NP-BOS (1985).
- [32] N. Pietralla, P. von Brentano, R.-D. Herzberg, U. Kneissl, N. Lo Iudice, H. Maser, H. H. Pitz, and A. Zilges, *Phys. Rev. C* **58**, 184 (1998).
- [33] D. D. Warner and R. F. Casten, *Phys. Rev. Lett.* **48**, 1385 (1982).
- [34] P. O. Lipas, P. Toivonen, and D. D. Warner, *Phys. Lett. B* **155**, 295 (1985).
- [35] P. Humby, A. Simon, C. W. Beausang, J. M. Allmond, J. T. Burke, R. J. Casperson, R. Chyzh, M. Dag, K. Gell, R. O. Hughes *et al.*, *Phys. Rev. C* **94**, 064314 (2016).